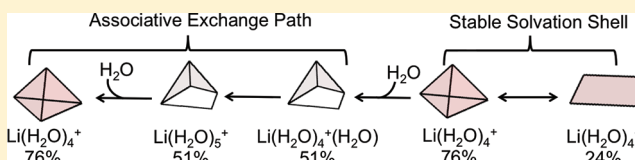


Novel Analysis of Cation Solvation Using a Graph Theoretic Approach

Barbara Logan Mooney,[†] L. Rene Corrales,^{*,†} and Aurora E. Clark^{*,‡}[†]Department of Chemistry and Biochemistry, University of Arizona, Tucson, Arizona 85721, United States[‡]Department of Chemistry, Washington State University, Pullman, Washington 99164, United States

S Supporting Information

ABSTRACT: A new method for analyzing molecular dynamics simulation data is employed to study the solvent shell structure and exchange processes of mono-, di-, and trivalent metal cations in water. The instantaneous coordination environment is characterized in terms of the coordinating waters' H-bonding network, orientations, mean residence times, and the polyhedral configuration. The graph-theory-based algorithm provides a rapid frame-by-frame identification of polyhedra and reveals fluctuations in the solvation shell shape—previously unexplored dynamic behavior that in many cases can be associated with the exchange reactions of water between the first and second solvation shells. Extended solvation structure is also analyzed graphically, revealing details of the hydrogen bonding network that have practical implications for connecting molecular dynamics data to ab initio cluster calculations. Although the individual analyses of water orientation, residence time, etc., are commonplace in the literature, their combination with graphical algorithms is new and provides added chemical insight.



INTRODUCTION

Aqueous solvation of metal ions plays a central role in the chemical mechanisms of biological signaling, in the bioavailability of toxic elements within the environment, in the design of new catalysts, in extraction processes, and in many phenomena relevant to technology.^{1–7} One of the most important features of solvation is the structural organization of water about the ion, which includes the positions of the O-atoms and the influence of the ion upon the water's H-bonding network. The former can be characterized using difficult X-ray and neutron diffraction methods,^{5–14} while dielectric relaxation spectroscopy, nuclear magnetic resonance (NMR), and ultrafast infrared spectroscopy can help elucidate perturbations in H-bonding relative to the bulk.^{7,15,16} Isotopic labeling⁵ and various other analyses within NMR can also be used to study the dynamics of the solvent shell, including the mechanisms and rates of solvent exchange.^{17–20} Despite these capabilities, there remain experimental limitations such as high concentration requirements, which introduce counterion effects (or ion pairing) and make the presence of bulk water questionable.

Computer simulations have thus played an important role within the field and have helped to elucidate a number of features and trends in solvation properties as a function of the ion charge and radius.^{21–33} For example, in a given charge state, the $\text{M}-\text{OH}_2$ interaction typically increases with decreasing ionic radius.^{21,34} As such, larger ions may accommodate more waters in their first solvation shell, and those waters are typically more labile and have a shorter residence time than around smaller ions. The structure of the first solvation shell about an ion is typically interpreted in terms of the polyhedral geometries that are adopted by the O-atoms of water. Though often described in the literature by a single average

configuration, the polyhedral structure is not static and need not be symmetric. The $\text{M}-\text{OH}_2$ distances within the first shell may not be all equal, and the number of solvating H_2O (referred to as the coordination number—CN) may be a time average of two (or more) values.³⁵ Structural order within the concentric solvation shells, as defined by the orientation of the H_2O dipoles relative to the $\text{M}-\text{O}$ bond, increases with the surface charge density of the ion.

The above is based largely on analyses of pair distribution functions (PDFs), coordinate transformations, and angular distribution functions designed to derive an averaged picture of solvation from statistical mechanical data. Yet, many properties exhibit dynamic behavior that is not straightforward. The effects of ions on the viscosity of aqueous salt solutions are considered to be related to the ability of the ion to alter the (bulk) H-bonding and tetrahedral arrangement of water (the “structure-maker/structure-breaker” concept),⁷ and the molecular origins of the Hofmeister series^{36–39} continue to be a subject of intense debate. Further, while the exchange of water between the first and second solvation shells is the simplest chemical reaction that the aqueous metal ion can undergo, the classification and identification of exchange mechanisms using both experimental and theoretical methods is challenging. Like the shape and size of the first solvation shell, the mechanism of exchange is a fundamental aspect of the ion–water interaction. While the behavior of the aqueous ions under different pressure and temperature regimes can probe exchange mechanisms,⁵ the exact structure of the reaction intermediates must be inferred,

Received: January 6, 2012

Revised: February 17, 2012

Published: March 14, 2012



leading to continued debate. To quote the review by Ohtaki and Radnai, “Discussions on the associative (A-) and dissociative (D-) mechanisms for solvent substitution reactions ... should disappear when (if) we could see the structure of the activated complexes ... in the solution”.³⁵

In this work, the recently developed *molecularRnetworks* graph theory analysis package^{40,41} has been applied to prototypical MD data of common metal cations to extract the shape(s) of the rearranging solvent shell and to derive new mechanistic insight. This analysis classifies the coordination polyhedra about ions “snapshot-by-snapshot” and allows correlations between the polyhedral arrangement and the solvation shell stability to further understand the exchange of water between solvation shells. The mechanisms of water exchange from this analysis are found to complement and in some cases independently validate recently reported mechanisms of water exchange for several ions. The relationship between the size and charge of the ion with the extent of H-bonding, the CN, the dipolar tilt of solvating H₂O, the solvation shell structure, and the lability of solvating H₂O is also explored in finer detail than previously reported. Results from simulations of TIP3P water and the monovalent cations Li⁺, Na⁺, and K⁺, the divalent cations Mg²⁺ and Ca²⁺, and trivalent La³⁺ are presented.

METHODS

Simulations employed DLPOLY⁴² with 216 TIP3P water molecules and one of the following ions: La³⁺, Ca²⁺, Mg²⁺, K⁺, Na⁺, and Li⁺. Interaction parameters for the monovalent and divalent cations were taken from Aqvist⁴³ and from the force field of Kuta et al.⁴⁴ for the trivalent cation (Table 1). The

Table 1. Mixed Interaction Parameters for the M–O Pairs Used in This Work^a

ion	epsilon	sigma
Li ¹⁺	0.0545717	2.588428
Na ¹⁺	0.0212522	3.239362
K ¹⁺	0.00730612	3.943080
Mg ²⁺	0.377577	2.276258
Ca ²⁺	0.270665	2.76765
La ³⁺	4.82207×10^{-4}	5.120568

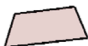




















^aEpsilon in kcal/mol, sigma in Å.^{43,44}

TIP3P model was chosen because prior studies of aqueous alkaline, alkaline earth, and rare earth ions using these model parameters have found M–OH bond lengths, CN, diffusion coefficients, and mean H₂O residence times in good accord with experimental values.^{25,30} Over the past decade, several hundred studies have used these parameters in similar nonpolarized aqueous media, and as such these data are representative of some of the most common MD data available for these ions. To handle the long-range forces, Ewald summation was used with a tightened tolerance of 10^{−08}. All simulations used a 1 fs time step. The initial neat water system was equilibrated within the NPT, NVT, and NVE ensembles each for 200 ps. Then, the density of the water subsystem was maintained at 1 g/cm³, the ion inserted, and a 200 ps equilibration in the NVT ensemble was carried out followed by 100 ps in the NVE ensemble to test stability at the target average temperature of 298 K. For each ion, there followed three 1 ns production runs. Data were collected from the production runs at a rate of once every 25 time steps for a total of 40 000 snapshots per 1 ns run.

Data analysis utilized the recently developed series of R-scripts *molecularRnetworks*.^{40,41} This analysis is dependent upon setting radial cutoffs that define the concentric solvation shells about the ion. This is one of the most important and least discussed features of solvation that inherently impacts all subsequent analyses of solvation structure. Most MD analyses utilize the minimum of the ion–water PDF, which is an average representation of the boundary between solvation shells. However, instantaneously at any one snapshot there can be H₂O migrating in and out of solvation shells, which can lead to false inclusion or exclusion of H₂O relevant to solvation. *molecularRnetworks* minimizes this issue by determining the distance at which the changes in the identity of the water molecules within the solvation shells are at a minimum (the minimum crossing distance—MCD). At the MCD, the waters “escape” the fewest number of times, as would be expected for H₂O experiencing the full electrostatic potential of the ion, and enter the fewest, as would be expected in the presence of a barrier to exchange. The CN and the average time that H₂O spent inside the first shell, termed the mean residence time (MRT), were then determined. The MRT of the first solvation shell waters was calculated through the introduction of a tolerance time, *t*^{*}: any molecule that does not leave the hydration shell for a time longer than *t*^{*} without returning back to the first shell is treated as not having left at all.³⁴ The introduction of *t*^{*} reduces issues associated with sampling and the time scale of rattling motions of H₂O near the MCD. A *t*^{*} value of 0.5 ps was used, amounting to 20 snapshots with 25 fs between each snapshot. Such a short *t*^{*} value is also supported in recent work by Laage and Hynes.⁴⁵ Exchange reactions were identified as those changes in CN that lasted less than 0.5 ps in duration that were not immediately preceded by another CN change less than 0.5 ps in duration: i.e., only the first exchange of a series was considered, such that the events were separated in time and distinct from one another. An increase in CN classifies the reaction as associative, while a decrease in CN is considered dissociative. Interchange reactions were identified as changes in the shell membership list without concurrent change in CN. This definition is simplified relative to that used in prior work (e.g., ref 46) but allows a consistent treatment of exchanges even in the face of apparently complex reaction dynamics (vide infra). The H₂O dipole orientations (angle of the H₂O dipole vs the O → M^{x+} vector) were also calculated and cross-correlated with radial distance to observe the influence of the ion on H₂O orientation and to examine reorientation during exchange. A value of 0° indicates perfect alignment with the O → M^{x+} vector.

molecularRnetworks utilizes the PageRank analysis algorithm⁴⁷ to create graphs of the polyhedral skeletons of the closest N waters about an ion. PageRank (PR), most famously used by Google to evaluate the importance of Web sites on the Internet, is used here as a descriptor of H-bonding structure and is unique to this toolkit. A graph is a mathematical object where individual points, or vertices, are joined by edges. In this case, each water O-atom is considered a vertex, and its nearest-neighbor atoms (and the connection to the solute) form an edge. The calculated PageRank (PR) of the ion based on the first solvation shell are then matched to a library of the associated values of known polyhedra, enabling rapid snapshot-by-snapshot identification of the coordination environment. The performance of the method in its ability to match structures is discussed in the Supporting Information. Two to five identifiable polyhedra are available for each CN (Table 2).

Table 2. Relevant Polyhedra As a Function of Coordination Number (CN)

CN	Relevant Polyhedra				
4	 square (S)	 tetrahedron (Td)			
5	 square pyramid (SPy)	 triangular bipyramid (TBP)	 wedge (W)		
6	 octahedron (O)	 pentagonal pyramid (PPy)	 trigonal prism (TP)	 capped SPy (CSPy)	
7	 capped octahedron (CO)	 augmented TP (ATP)	 cut dodecahedron (CDo)	 pentagonal bipyramid (PBP)	 cut cube (CC)
8	 biaugmented TP (BATP)	 dodecahedron (Do)	 square antiprism (SAP)		
9	 monocapped SAP (MCSAP)	 triaugmented TP (Tri-ATP)			
10	 bicapped SAP (BCSAP)	 tetra-augmented TP (Tetra-ATP)			

While the majority is recognizable structures with regular polygon faces, in the case of extreme deformation, structures that are adopted during dramatic shape changes in the solvation shells should be identified. These “pseudopolyhedra” were devised for shapes that are not a convex body with regular faces. The wedge (W) is an example of an improper pseudopolyhedron that nevertheless contributes to the coordination geometry of two ions in this study. It consists of a triangle with a connected pair of waters above, one of which is connected to the two points of the base of the triangle and the other which is connected to the top of the triangle (Table 2). Among the 10-coordinated structures, seven different tetra-augmented trigonal prisms (Tetra-ATP) have been investigated that vary in the point of attachment of the new vertex to the underlying Tri-ATP polyhedra. Of these, just one accounts for the majority of tetra-ATP observations, and it alone is discussed. The identified polyhedra were assigned to one of five categories: stable coordination, oversaturated and stable, undersaturated and stable, oversaturated exchange intermediate, or undersaturated exchange intermediate. The distributions of polyhedra within each category were then compared to

determine the relationship of a particular polyhedron with stability or exchange within the first solvation shell.

To explore the relationship between polyhedra, exchange, and H-bonding, a graph of the entire water network for each snapshot is constructed. In these graphs, the edges are not simply nearest neighbors *but H-bonds*. The criteria used to define a H-bond are: (1) the O-atom of one molecule lies within 2.5 Å of a H-atom on another, and (2) the associated O⋯H–O angle was no smaller than 150°. The sensitivity of the analysis to this definition is discussed in the Results and Discussion section. Borrowing the language of graph theory, the *mean degree* of H₂O within the first solvation shell is defined as the average number of H-bonds (over all snapshots) plus one for the connection to the ion. This definition explicitly incorporates the ion into the network and thus differs from that commonly used in investigations of H-bonding near a solute. The relationship between the distance from the ion and the mean degree of H₂O was examined using *t* tests and clustering algorithms implemented in *molecularNetworks*.

RESULTS AND DISCUSSION

The MD results presented here are in good agreement with prior theoretical and experimental studies using the same potentials and simulation protocols (vide infra). The radial cutoffs and CNs for each ion are presented in the Supporting Information. For the mono- and divalent cations, the peaks in the PDFs are in exact agreement with Aqvist and prior MD studies. The results from our analyses are arranged as follows. First, the coordination environments of the ions are presented, and then water orientation and hydrogen bonding are examined, followed by a description of exchange reactions.

Coordination Environment. Analysis of statistical mechanical data typically relies upon the PDF to determine the CN. While it is possible to use the total O–M–O angular distribution to resolve the data into the dominant polyhedral shapes adopted within the first solvation shell, to date there has been no well-defined algorithm for obtaining the relative contributions of the polyhedra nor their lifetimes. This has prevented further study into correlations between the polyhedra and aqueous reactivity.

As presented in Table 3, the Li^+ ion is 4-coordinated 66.0% of the time and 5-coordinated 32.8% of the time to give a mean CN of 4.35 ± 0.50 . This is in good agreement with ab initio and experimental studies that give a CN of 4 (with a tetrahedral geometry);^{48,49} other classical simulations indicate 4 or a mix of 4- and 5-fold coordination.^{29,50,51} During the time when it is 4-coordinate, a tetrahedral geometry (Td) is observed 40.3% of the time and a square planar (S) geometry 24.0% of the time, with a “broken tetrahedral” shape observed 35.8% of the time.⁵² When it is 5-coordinated, square pyramidal (SPy) and wedge (W) geometries are observed with nearly equal frequency (45.9% and 53.0%, respectively). The transitions between coordination environments arise from natural fluctuations in the M–O distances and deformations in O–M–O angles and are a first-order process. Fitting the lifetimes of the predominant polyhedra (S, Td, “broken” Td, SPy, and W) to an exponential distribution results in half-lives of 38.6, 30.0, 24.3, 44.2, and 58.8 fs, respectively (Table 3). Such short dynamics are a result of the purely electrostatic interaction between the ion and water and time scale of the O–M–O bending vibrations that enable one polyhedron to deform into another. Moreover, the minimum distance for each H_2O to move to transform between a given N-vertex polygon is quite small (tenths of Å). Further, a prior review on the dynamics of bulk water has pointed out that “on very short time scales (<200 fs), the OH/OD group can show a limited free rotation (libration) while keeping the donated H-bond intact”.⁵³ Thus, it is possible for the polygon lifetime to be shorter than a typical H-bond within bulk water. The rapid sampling of configurations within the first solvation shell is captured well by the *molecularRnetworks* analysis; however, the resulting polyhedral distributions differ from other methods of characterizing the solvation shell geometries. For instance, the symmetry axis method in ref 23 yields polyhedron lifetimes orders of magnitude longer than in this work due to the assumption of a single, highly symmetric shape for each CN; as such, that analysis reveals only the most dramatic shape transformations which occur on the time scale of water exchange. A key feature of this analysis is that more subtle, distorted structures that could be viewed as intermediates in dramatic shape changes are also identified.

Table 3. Summary of MD Results for the First Solvation Shell^{a,b}

ion	CN	CN (%)	% p	τ	mean degree	MRT
Li^+	4	66	Td, 76 S, 24	30, 24.3 38.6	2.53	$11.29 \pm .58$
	5	33	SPy, 46 W, 53	44.2 58.8	2.57	
Na^+	5	37	SPy, 47 W, 48	45.3 68.9	2.67	$9.86 \pm .18$
	6	58	TBP, 3 O, 38 CSPy, 20 DO, 21	38.7 37.8 32.2 34.5	2.70	
K^+	6	44.8	CSPy, 26 O, 26.5 PP, 17	NA NA NA	2.87	24.46 ± 1.37
	7	30	CDo, 29 PBP, 31 ATP, 23	NA NA NA	2.91	
Mg^{2+}	6	100	O, 78.6 DO, 21.1	91.7 13.5	2.61	--
Ca^{2+}	7	38	PBP, 62.6 CC, 22.1 CDo, 15.1	71.2 46.8 27.1	2.48	60.01 ± 8.58
	8	61	SA, 45.6 BATP, 42.6 Do, 11.8	108.2 56.4 32.8	2.43	
La^{3+}	9	91	MCSAP, 15.9 TATP, 84.1	30.1 156.9	2.52	194.2 ± 31.9
	10	9	BCSAP 85.6 TrATP7, 11.4	114.8 34.1	2.48	

^aThe percent observation of each coordination number (CN), dominant percent polyhedra for each CN (% p), the polyhedron half-lives (τ in fs), the mean degree of the solvating waters (average number of H-bonds +1), and mean residence time (in ps) are presented. ^b $t^* = 2$ ps for Li and 0.5 ps for all other ions; average: mean \pm standard deviation.

Recent theoretical and experimental work has indicated a 5 or 4 + 1 coordination state^{26,29,55} for Na^+ ; however, many MD studies have observed 6-coordinate Na^+ . X-ray scattering studies also typically assume 6-coordination with the maximally symmetrical octahedral configuration. In this work, the Na^+ ion is predominantly 6-coordinated (57.8%) and 5-coordinated (37.4%), resulting in a mean CN of 5.64 ± 0.57 . The dominant polyhedra adopted for 5-coordination is the W (47.5%), followed closely by the SPy (46.6%), with occasional observations of the TBP (3.4%). When 6-coordinated, the octahedron (O) is dominant (38.4%), followed by a distorted octahedron (21.1%) and a “capped” square pyramid (CSPy) (20.2%). The pentagonal pyramid (PPy) and triangular prism (TP) are also observed 8.8% and 7.9% of the time, respectively. Having the largest ionic radius, K^+ is found in coordination states ranging from 3 to 10, with 6 (observed 44.8% of the time) and 7 (30.0%) the most common, to give a mean CN of 6.25 ± 0.87 . Prior theoretical and experimental studies of K^+ suggest a weak $\text{K}^+ - \text{OH}_2$ interaction which leads to an amorphous shell. This is further supported by the polyhedral distributions.¹² When 6-coordinated, the dominant polyhedra

observed are the O (26.5%) and the CSPy (26.3%). The PPy (17.2%) and TP (13.4%) are also frequently observed. Relative to the 6-coordinated Na^+ ion, both the O and the distorted O (8.9%) are significantly reduced in prevalence. Thus, in comparison to Na^+ , the solvation structure about K^+ has much less tendency toward an octahedral environment. When 7-coordinated, the pentagonal bipyramid (PBP, 30.9%) and cut dodecahedron (CDo, 29.3%) structures are most frequently observed. The augmented triangular prism (ATP, 23.0%) and cut cube (CC, 13.0%) are also observed. Very rapid transitions are observed between configurations, and during a 1 ns run only one CN interval lasted longer than 100 snapshots (2.5 ps), preventing the calculation of the polyhedra half-lives.

Experimentally, the stable 6-coordinate solvation shell about Mg^{2+} is well established.⁷ This is reflected in the MD simulations, where a CN of 6 is observed for the entire length of the simulation.^{7,37} Despite this stability, the first solvation shell is quite dynamic, twisting and evolving even though the solvating waters do not dissociate. Both octahedral and distorted octahedral configurations are observed (78.6% and 21.1%, respectively), with half-lives of 91.7 and 13.5 fs, respectively. The octahedron half-life is more than 2.5 times as long as that observed in Na^+ and K^+ . The solvation of Ca^{2+} is more varied, as it is observed in 7- and 8-fold coordination states, with 6-fold coordination rare (<1%) and 9-fold transient. The ion is 7-coordinated 37.9% of the time and 8-coordinated 61.2% of the time, for a mean CN of 7.60 ± 0.51 . Experiment finds a CN of 8 for Ca^{2+} , with evidence of a square antiprism (SAP) configuration.^{56–58} This is supported by the *molecularRnetworks* analysis wherein the predominant polyhedra are the square antiprism (SAP, 45.6%), biaugmented triangular prism (BATP, 42.6%), and dodecahedron (Do, 11.8%) during the times when Ca^{2+} is 8-coordinate. This is in good agreement with recent work by Lim et al.,⁵⁸ who used the total O–M–O angular distribution of the first-shell waters to infer nearly equal contributions of the SAP, the biaugmented trigonal prism (BATP), and Do. Classical simulations also typically find a population of 7-coordinated ions for Ca^{2+} .⁷ In this case, the predominant polyhedra observed are the pentagonal bipyramid (PBP, 62.6%), the cut cube (CC, 22.1%), and cut dodecahedron (CDo, 15.1%). The La^{3+} ion is predominantly 9-coordinated (91.4%) and 10-coordinated the remainder of the time for a mean CN of 9.09 ± 0.28 . This is in excellent agreement with the literature that finds a 9-fold coordination structure.⁵⁴ When 9-coordinate, the dominant polyhedron is the triaugmented triangular prism (TATP, 84.12%), while a monocapped square antiprism (MCSAP) is also observed (15.88%). When 10-coordinated, the bicapped square antiprism (BCSAP) is dominant (85.58%) with various tetracapped square antiprisms (tetra-ATPs) present the rest of the time.

Water Orientation and Hydrogen Bonding. The orientation of H_2O and its ability to form H-bonds are intimately linked. Examination of the dipole orientations and mean degree of the waters in the first and second solvation shells yields new information regarding their behavior within specific coordination environments. Among the monovalent ions, examination of the mean degree as a function of metal–water distance reveals a steady increase in H-bonding with increasing bond length within the first solvation shell, with the mean degree highest for those waters farthest from the ion, yet still coordinated (Figure 1a). This distance corresponds to the minimum in the M–O pair distribution function (Figure 1 inset), which occurs at 2.88, 3.23, and 3.63 Å, for Li^+ , Na^+ , and

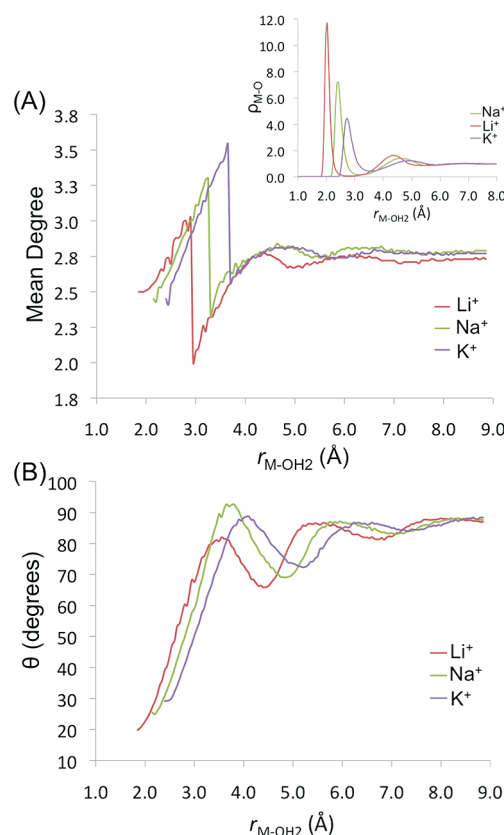


Figure 1. (A) Mean degree of the waters within the 1st and 2nd solvation shell as a function of M–OH₂ distance for monovalent cations. (B) Mean dipole angle of the waters within the 1st and 2nd solvation shell waters as a function of the M–OH₂ distance for monovalent cations. Cation–water pair distribution function inset.

K^+ , respectively. A sharp drop at the boundary of the first and second solvation shells is due to the change in the number of connections for the first and second solvation shell waters. Recall that the mean degree in the first shell is the number of H-bonds plus the connection to the ion, while the mean degree is equivalent to the number of H-bonds in the second solvation shell and beyond. This analysis does indicate that, the boundary waters are connected to the network to less of an extent than are waters slightly farther into the second solvation shell. This is indicated by the increase in mean degree for individual H_2O in the second shell as a function of metal–water distance, which reaches a plateau that smoothly transitions into the converged bulk values of 2.7 and 2.8 beyond 6 Å. To test the importance of the prescribed definition of a H-bond upon these data, a broader angle criterion was examined. Allowing the associated O...H–O angle to be no smaller than 120° uniformly increases the mean degree by ~1 unit (see Supporting Information). Thus, while the quantitative data may shift, the qualitative conclusions drawn here remain applicable across multiple H-bond definitions.

Similar plots of the dipole angles complement the mean degree data (Figure 1b). The H_2O that hydrates monovalent ions has angles that begin between 20° and 30° and smoothly increase within the first solvation shell. The dipole angles decrease for the waters in the second solvation shell that are close to the boundary but then again slowly increase as a function of distance until a peak is reached at the edge of the shell boundary. The angles plateau beyond 6 Å; in the absence

of an orienting force, the expectation value of the angular orientation with respect to the center of the simulation box is 90° .

An overall increase in the surface charge density of the di- and trivalent ions⁵⁹ leads to significantly different solvation behavior (Figure 2). Instead of an increase in the number of H-

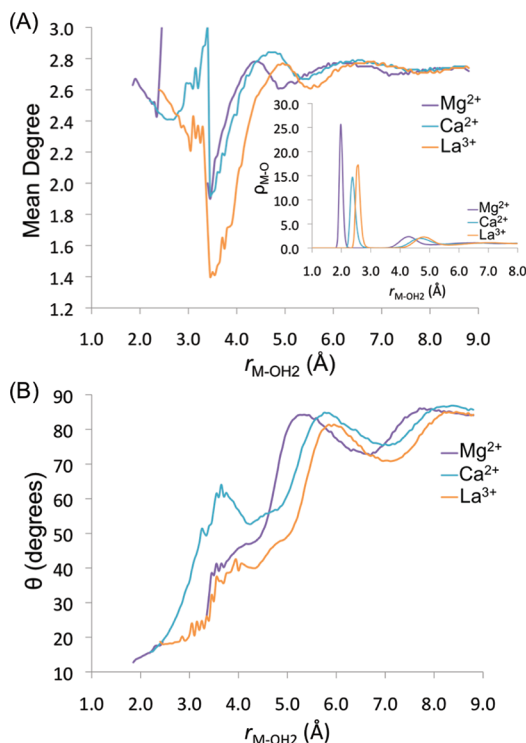


Figure 2. (A) Mean degree of the waters within the first and second solvation shell as a function of M–OH₂ distance for di- and trivalent cations. (B) Mean dipole angle of the waters within the first and second solvation shell waters as a function of the M–OH₂ distance for di- and trivalent cations. Cation–water pair distribution function inset.

bonds as a function of distance within the first solvation shell, a decrease is observed until the boundary of the first and second solvation shell is reached (indicated by the minima in the M–O pair distribution function; Figure 2 inset), where the mean degree finally begins to increase (Figure 2a). This behavior makes chemical sense as the H₂O closest to the ion is more highly oriented than in the monovalent ions (with dipole angles $<20^\circ$) and there is much less rotational flexibility for the first shell waters with increasing M–O distance (Figure 2b). Indeed, among the di- and trivalent ions, the strong ion–dipole interaction aligns H₂O in both the first and second solvation shells and increases H-bonding between the two. At the boundary of the first and second solvation shells about Mg²⁺, a large break in the mean degree and water dipole data occurs, caused by the first shell waters residing within a small distance range and the absence of exchange reactions between the two shells. A drop in the number of H-bonds is observed for the boundary waters in the second solvation shell for all ions, and then a steady increase in mean degree is observed at farther distances. At 5–6 Å from the ion, another oscillation in mean degree is observed, indicative of a small perturbation in the H-bonding network that would occur in a third solvation shell prior to bulk behavior at 7–9 Å. Commensurate with the H-bonding data, there is a steady increase in dipole angle within

the second solvation shell until a maximum is reached at the edge of the shell boundary. As in the mean degree data, a second oscillation is observed in the dipole angle between 6 and 9 Å that indicates some orientational structure from a third solvation shell.

Statistical analyses implemented in *molecularRnetworks* indicate that there is a significant change in both mean degree and dipole orientation when the ion changes CN. However, for a given CN, comparison of the two most significant polyhedra reveals no correlation with the shape of the first solvation shell. Consider the first shell about Li⁺, wherein the solvating H₂O adopts a dipole angle of 23.35° for Li(H₂O)₄⁺ and 29.24° for Li(H₂O)₅⁺. The small angle indicates significant orientational ordering that weakens with increasing CN. Concomitantly, there is a small increase in H-bonding within the first shell waters as the CN is increased from 4 to 5, with an average mean degree for the first shell waters of 2.53 in Li(H₂O)₄⁺ and 2.57 in Li(H₂O)₅⁺ (Table 3). Application of Student's *t*,⁶⁰ a statistical test for comparing the means of two populations, reveals that the difference in the means is statistically significant, with a *p*-value $<2.2 \times 10^{-16}$; this implies that the H₂O in Li(H₂O)₅⁺ engages in more H-bonding. Further *t* testing to compare the closest water's mean degree when 4-coordinated with the closest water's mean degree when 5-coordinated reveals that the CN has an insignificant effect on the H-bonding of waters 1–3, but the fourth and fifth closest waters have different H-bonding depending on the CN. Student's *t* applied to the 4-coordinate tetrahedron (Td) vs square (S) and the 5-coordinate wedge (W) vs square pyramid (SPy) exhibit no significant differences in H-bonding. This is to be expected given that the polyhedron lifetime is much faster than fluctuations of individual H-bonds. In combination with the data shown in Figure 1, this analysis indicates that the extent of H-bonding and water orientation in the first solvation shell are dominated solely by the M–OH₂ bond distance and CN.

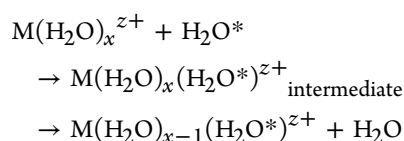
Similar conclusions are drawn from the analysis of the remaining cations; however, interesting differences in solvation properties within the first shell are revealed. The behavior of Na⁺ is quite similar to Li⁺; however, for both Na(H₂O)₅⁺ and Na(H₂O)₆⁺ the farthest water molecule has a significant increase in mean degree relative to the other waters. This holds even for the octahedral geometry of Na(H₂O)₆⁺, in contrast to expectations based on symmetry. In aqueous K⁺, waters in the first solvation shell are characterized by significantly more H-bonding than in the shells of either Li⁺ or Na⁺. The K(H₂O)₅⁺ waters have a mean degree of 2.82, which increases to 2.87 in K(H₂O)₆⁺ and 2.91 in K(H₂O)₇⁺ (Table 3). The differences in the means are statistically significant with *p* values $<2.0 \times 10^{-16}$. As observed in Figure 1a, the slope of the increase in mean degree as a function of distance is less steep than in the other monovalent ions. This is revealed to be due to an increase in the population of waters with three and four H-bonds, indicating that they rotate more freely and thus accept H-bonds more readily. These H₂O also exhibit the weakest ordering in terms of their dipole alignment with the O → K⁺ vector, having an average angle spanning 38.9° when 5-coordinated to 48.4° when 7-coordinated, in good agreement with the dipole tilts reported by Soper and Weckström.¹² In sharp contrast, the solvating H₂O about Mg²⁺ exhibits the strongest dipole alignment of all the ions with an average angle of 14.4° (Figure 2b). The dipole alignment of H₂O about Ca²⁺ and La³⁺ is also significant, with angles

between 17.0 and 20.0°. The strong rotational alignment decreases the overall H-bonding for those waters in the first solvation shell about the di- and trivalent ions. Moreover, while the differences in H-bonding between different CNs are statistically significant for all ions, as higher CN values are approached, the H₂O orientations become more similar. The H₂O in La(H₂O)₉³⁺ has a mean degree of 2.52, while those in La(H₂O)₈³⁺ are 0.04 smaller; yet, the mean dipole angles are statistically the same (18.2° for La(H₂O)₉³⁺ and 18.4° for La(H₂O)₁₀³⁺, with $p = 0.2$).

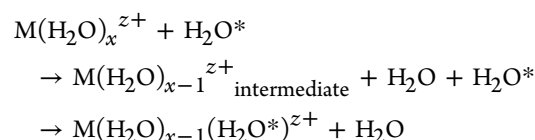
Using the MCD to define the second solvation shells leads to 15.0 ± 1.9, 17.0 ± 2.0, and 18.7 ± 2.1 waters for the monovalent Li⁺, Na⁺, and K⁺ ions, respectively. These H₂O have weak orientational order relative to the first shell with dipole angles that span 65–90°. In contrast, the di- and trivalent ions have second solvation shells that are nearly as ordered as the first solvation shells about the monovalent ions. The mean number of H₂O molecules in the second solvation shell about Mg²⁺ is 13.8 ± 1.5, while Ca²⁺ has 17.7 ± 1.9 and La³⁺ has 18.6 ± 1.7. These values represent the traditional view of the second solvation shell; however, if one considers a second shell to be made up of only those waters that are H-bonded to the first shell, then the mean degree indicates that less than half of the H₂O that surrounds the first shell is actually connected to it via H-bonds. In the case of Li⁺, 6–8 H₂O in the second shell are H-bonded to the first, while 8–10 and 9–13 H₂O have this connectivity for Na⁺ and K⁺, respectively. Divalent Ca²⁺ has ~11–12 H₂O in the second solvation shell that are H-bonded to the first shell, while La³⁺ has 13–15; however, it is Mg²⁺ that has the largest proportion of second-shell waters H-bonded to the first (9–10 H₂O out of the total 13.8), which illustrates the tightness of the shell structure that has long been observed in both experiment and theory.^{7,61} The H-bond connectivity between solvation shells has important ramifications for the study of ion solvation using gas-phase ab initio cluster models. Within that approach, significant effort has been dedicated toward determining the appropriate number of solvating waters in the second shell (which are necessarily H-bonded to the first shell waters), to reproduce the key solvent interactions needed to accurately predict thermodynamic properties of solvation.^{62,63}

Exchange Reactions: Implications from Polyhedral Structure. Water exchange between the first solvation shell and either the second shell or bulk is the simplest chemical reaction an aqueous metal ion can undergo, forming a fundamental basis of our understanding of the behavior of aqueous ions. The trends in the mechanisms and rates of water exchange follow trends in ion reactivity and are related to aqueous ligand complexation reactions and ligand exchange. The mechanisms of water exchange can be classified as associative (A), dissociative (D), or interchange (I). The first two are classified by intermediates that are either oversaturated (A) or undersaturated (D) relative to the starting complex.

Associative (A):



Dissociative (D):



where M represents the metal cation with a charge of $z+$. Interchange mechanisms have minimal activation barriers for both association and dissociation and may be subdivided into I_A (associatively activated interchange) and I_D (dissociatively activated interchange) mechanisms, depending on the (radial) distance at which the entering and exiting particles are equidistant from the central ion, with $r_{\text{IA}} < r_1 < r_{\text{ID}}$. Factors that contribute to a preferred exchange pathway include the rigidity of the first and second solvation shells, the extent of thermally induced fluctuations within the system, and the magnitude of the activation barrier for association/dissociation.⁶⁴

The definition of what constitutes an exchange reaction within a MD simulation is subject to some variability. One way to define an exchange is by the direct (visual) examination of particle distance trajectories. With this method, a single CN is assumed. The first change from that coordination number, whether it be the arrival or departure of a H₂O molecule, marks the beginning of the exchange event. Note that some methods⁶⁵ require the exchanging water to enter from/exit to the bulk, while others do not. The end of the exchange process is the return to the original coordination state. Mechanistic classification (A, D, or I) may also be based on the duration of the exchange interval and the distance from the ion at which the incoming/outgoing particle trajectories cross. Particular difficulties arise from this method of mechanistic classification. First, there is some arbitrariness in the cutoffs used to define the exchange mechanism (e.g., the delineation between associative vs associatively activated interchange mechanisms). Second, within the course of the MD simulation, multiple transient associations/dissociations of water molecules may happen in succession during the period of under- or oversaturation. The latter point is particularly relevant for the monovalent cations where it complicates the classification of the exchange mechanism, such that they are often merely referred to as “complex” exchange processes. Finally, a requirement that an exchanging H₂O must come from some set distance from the ion is difficult to implement from an algorithmic perspective.

In this work, the definition of exchange is simplified to include only those changes in CN which are temporary, less than t^* in duration. This is the opposite of the direct method of Hofer et al.,⁶⁵ as here the intervals which are greater than t^* are considered stable runs of an over- or under-saturated coordination number, such that multiple coordination numbers are allowable for each ion. Thus, the data are separated so that the distributions of polyhedra can be compared and the polyhedra that are associated with shell instability can be determined. In those cases where multiple brief coordination number changes happen in sequence, only the first is examined, to look for the initial shifts in geometry that may enable an exchange process. No requirement is placed upon whether the exchanging H₂O comes from the bulk, and as such waters that participate in exchange from the second solvation shell are counted. This necessarily means that exchange will not be a

diffusion-limited process, and in fact there are often many more exchange events than would be anticipated from $1/\text{MRT}$.

Figure 3 illustrates the definitions of aqueous exchange used within this work through examination of the trajectories of 8

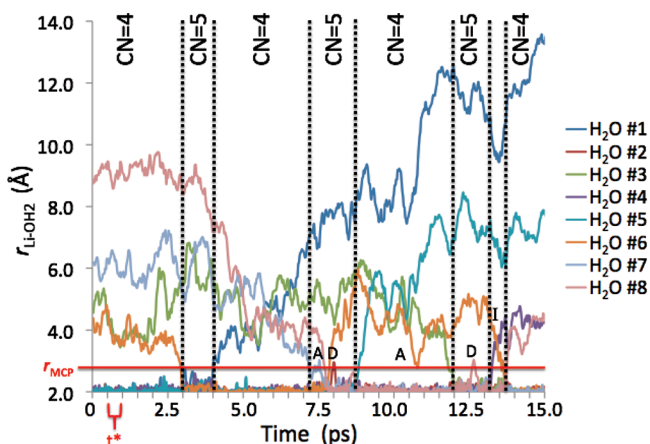


Figure 3. Trajectories of 8 associated water molecules about Li^+ over a 15 ps time frame. Associative (A), dissociative (D), and interchange (I) exchange pathways are identified according to *moleculaRnetworks*.

water molecules that spend some time in the first solvation shell about Li^+ during a 15 ps time frame. Consider the time interval from 0 to 3 ps: a water molecule residing in the second shell (H_2O #6) approaches an initially 4-coordinated Li^+ , adding to the shell to create a 5-coordinated species that is stable between 3.0 and 4.0 ps. As the shell remains 5-coordinated for >0.5 ps (t^*), within this work the process is counted as a water addition reaction. Water #1 migrates out of the first solvation shell at 4 ps to create a stable 4-coordinated species; however, at 7 ps a very complex process begins in which two waters (H_2O #7 and #8) simultaneously approach the first shell from the second, expelling H_2O #6 as they enter to create a 5-coordinated species. This could be termed an interchange and also an associative mechanism because the CN increases from 4 to 5; however, it is uncertain which of the two entering H_2O is associating and which is interchanging. *moleculaRnetworks* identifies the initial paired entry at ~ 7.6 ps as an associative exchange. The 5-coordinated species is relatively stable until 8.8 ps, with one dissociative exchange at 8.0 ps observed wherein H_2O #2 briefly escapes the first solvation shell, only to pop right back in again. Inclusion of this event is justified as an exchange by noting that we are using the concept of exchange to identify regions of instability in the coordination shell to identify unstable polyhedral geometries, and the escape of H_2O #2 represents an instability. At approximately 8.6 ps, H_2O #5 leaves the first solvation shell to create another stable complex with a CN of 4 that has a lifetime of ~ 3 ps. One brief associative exchange is observed at ~ 10.8 ps involving H_2O #6 (which has remained in the second solvation shell since it dissociated from the first shell at 7.6 ps). At 12.0 ps, H_2O #3 adds to the first solvation shell from the second; however, this 5-coordinated species is somewhat unstable, as at 12.6 ps H_2O #8 is involved in a dissociative exchange. An interchange reaction is initiated at ~ 13 ps, as H_2O #6 comes in from the second solvation shell at the same time that H_2O #4 leaves the first shell. Shortly thereafter, H_2O #8 dissociates from the cation and enters the second solvation shell.

In comparison to the definition described above, if only those reactions where a H_2O from the bulk are considered, then the exchange reaction from 7.6 to 13.6 ps becomes the sole associative exchange process. Indeed, 1 exchange event in 15 ps leads to a chemically reasonable number of 67 exchanges per nanosecond. Alternatively, if a fixed CN scheme is adopted, then the processes from 3 to 4, 7 to 8.6, and ~ 12 to 13.5 ps would be considered exchanges, two of them with “complex” mechanisms. Figure 3 clearly shows how the method employed in this work simplifies the classification of the observed complex exchange dynamics: when H_2O enter or leave and stay that way, they are stable; when H_2O enter or leave and quickly depart or return, they are unstable. From a statistical point of view, for most ions, this yields sufficient snapshots in each category for a comparison of the water exchange reactivity as a function of polyhedral distributions.

Given that the polyhedral geometries of the first solvation shell have been determined, and the exchange events identified for each ion, it is a natural extension to examine potential correlations between polyhedron and exchange reactivity. To do this, the analysis must go beyond determining the frequency of observation of a given polyhedral shape and instead must compare those polyhedra associated with a state of over- or undersaturation of CN. The analysis first determines the distribution of polyhedra when the ion is in a stable coordination state ($t > t^*$). The distribution of polyhedra for the transient coordination states is then compiled ($t < t^*$). Finally, the underlying and overlying polyhedron of both stable and transient coordination states is determined. In the former, when N waters surround an ion, the closest $N - 1$ of them can be considered as forming an *underlying* polyhedron. Similarly, the closest $N + 1$ can be considered as forming an *overlying* polyhedron. It is our contention that there is chemical significance in examination of the under- and overlying polyhedral structures as they reveal those arrangements that are “pre-organized” to undergo an exchange event. Consider a 5-coordinated ion: the likelihood of this ion undergoing a dissociation and remaining in the lower coordination state may be greater if the closest four waters (which form the underlying polyhedron) are in a Td arrangement than if they are in a square planar arrangement since the most likely 4-coordinate polyhedral geometry is a tetrahedron. As for the overlying polyhedron, if the closest six waters form an octahedral shape, it may be more likely that an associative exchange (or addition reaction) occurs. While one cannot obtain causation from such a statistical correlation and it is difficult to quantify the statistical significance of the differences in the distributions, it nevertheless implicates the role of geometry in water exchange objectively and without reliance upon visualization tools to process the structural rearrangements. A complete table of all the polyhedral distributions discussed herein is presented in the Supporting Information. The remainder of this section is arranged as follows: for each ion, the mean residence time (MRT) of the first solvation shell is presented, followed by the number and classification of exchanges, the comparison of the polyhedral distributions for the A and D exchange events, and an overview of a putative chemical exchange process is described.

Mean residence times (MRT) of waters in the first solvation shell of Li^+ were calculated for three independent 1 ns runs and found to be 11.70, 10.62, and 11.54 ps, for an average MRT of 11.29 ± 0.58 ps (Table 3). For simplicity, the first 1 ns run is discussed, in which the Li^+ ion undergoes 238 exchanges, as

defined above. Of these, 128 were associative, 108 were dissociative, and 2 were interchange. Considering first the associative exchanges, in which water adds to $\text{Li}(\text{H}_2\text{O})_4^+$ to form a 5-coordinated transient intermediate, the dominant polyhedron for the intermediate is a W (51.4%) followed by the SPy (44.8%). The TBP appears 3.8% of the time. In comparison, when the Li^+ exists as a stable 4-coordinate species, if the geometry including the fifth closest water is examined, the overlying polyhedral distribution is quite similar: the W is observed 51.3% of the time, followed by the SPy at 39.5%, and the TBP at 9.2%. However, it is generally observed that the 4 + 1 geometry is not highly organized, as the overlying polyhedra are only identifiable 23% of the time. It is then plausible that the addition of a H_2O is more likely to occur once the 4 + 1 waters move into a W or SPy geometry, that is, they are preorganized for an association to occur. Conversely, an overlying TBP (trigonal bipyramidal) polyhedron appears less conducive to a stable addition process. The dissociative exchange from $\text{Li}(\text{H}_2\text{O})_5^+$ to create a 4-coordinate transient intermediate can be similarly examined. Here, the distribution of transient 4-vertex polyhedra mimics that of Li^+ as a stable 4-coordinate species, with the Td (40.3%), broken Td (34.1%), and square (S, 25.0%) observed. Yet, if the underlying polyhedra of the $\text{Li}(\text{H}_2\text{O})_5^+$ reactant is considered, the S and broken Td swap order (31.0% and 25.1%, respectively). Taken as a whole, the distributions suggest that the 5-coordinate structure is more likely to dissociate to form a 4-coordinate structure when the underlying polyhedron is Td or broken Td. This result makes sense in light of the fact that the broken Td has multiple sides that exceed the cutoff distance giving it a larger volume that encompasses more of the ion's surface area. On the other hand, H_2O dissociation when the underlying polyhedron is a square is disfavored. When the underlying polyhedron is a square, the geometry of the $\text{Li}(\text{H}_2\text{O})_5^+$ is a square pyramid, and dissociation of the water at the peak position likely leaves the ion overly exposed.

From a mechanistic standpoint, the primary CN for Li^+ is 4 and transitions to 5-coordination last on the order of a few picoseconds. Using the above information to infer the overall process of change, it is proposed that an entering H_2O moves into position along an edge of the dynamically evolving Td to form a W, which, as the Td fluctuates and opens up, may become a more stable SPy. The H_2O enters the shell and remains there until fluctuations drive the four closest waters to rearrange into a more tetrahedral arrangement and the furthest H_2O is spontaneously expelled. Compare this to the work of Loeffler et al.,⁶⁶ who also reported an associative mechanism for Li^+ , based on QM/MM MD umbrella sampling. They report from angular distributions that the (underlying) Td remains during the associative exchange event—a finding which our data support. Although the expulsion of the *cis* water is confirmed, the shape of the wedge is such that the entering H_2O comes between two corners of the Td, pushing those H_2O away from the ion, such that they may be the more likely to dissociate.

In the case of aqueous Na^+ , the MRTs are 9.65, 9.97, and 9.95 ps, with a mean of 9.86 ± 0.18 ps (Table 3). Although this is significantly shorter than the MRT given by Lee of 26.4 ps,²⁴ a check of our data reveals this to be related to our choice of t^* . The use of 1 ps as t^* increases the obtained MRT to 20.30 ps, and the use of 1.25 ps gives 27.60 ps. For both Na^+ and K^+ , the majority of CN intervals is short, and as such using the t^* method results in rejecting a large portion of them. Lee and

Rasaiah used exponential fitting to calculate their MRT, which may be interpreted as using a larger t^* value. The shortened MRT of Na^+ relative to Li^+ and the abundance of short coordination intervals explains the near doubling of observed exchange events (464) within a 1 ns simulation of aqueous Na^+ . Of these, 220 are classified as associative (CN from 5 to 6, some 6 to 7), 231 are dissociative (CN from 6 to 5 or 7 to 6), and 13 are interchange. Within the associative exchange events where a water adds to $\text{Na}(\text{H}_2\text{O})_5^+$, the transient 6-coordinated intermediate adopts O and distorted O geometries (26.0% and 8.4% frequency, respectively) as well as CSPy, TP, and PPy (27.7%, 16.7%, and 15.1%). Further, a second type of distorted O emerges (5.9%) that is rarely observed in the stable runs of 6-coordination (2.7%). This distribution is very different from that observed for stable $\text{Na}(\text{H}_2\text{O})_6^{+}$; however, it does bear strong similarities to the overlying polyhedra distribution of $\text{Na}(\text{H}_2\text{O})_5^+$, in which the CSPy is dominant (27.9%), followed by the PPy (13.9%), and the second distorted O (11.9%) is more prevalent than the TP and O (10.1% and 10.0%). Further, *moleculaRnetworks* determines the overlying polyhedra of $\text{Na}(\text{H}_2\text{O})_5^+$ over 99% of the time, suggesting that H_2O at the boundary of the first solvation shell are nearly always preorganized to participate in the associative process. This is in contrast to that observed for Li^+ , where H_2O are most likely to undergo addition once the thermal fluctuation of the boundary water molecules moved them into position. Just as interesting is that in the case of Li^+ the associative intermediate adopts the same geometry as a stable oversaturated species; thus, when the H_2O addition occurs it is likely to lead to a stable run of the oversaturated species. However, in Na^+ , the transient intermediate must rearrange for a stable period of $\text{Na}(\text{H}_2\text{O})_6^{+}$ to occur (i.e., the distorted octahedron must become the ideal octahedron). Within the dissociative exchange processes, H_2O is lost from $\text{Na}(\text{H}_2\text{O})_6^{+}$ to yield a 5-coordinated species that adopts a SPy (50.4%), a W (44.4%), and a TBP (5.2%). This polyhedral distribution is very similar to that found for the stable $\text{Na}(\text{H}_2\text{O})_5^+$ species and somewhat similar to the underlying polyhedral distribution of $\text{Na}(\text{H}_2\text{O})_6^{+}$. As observed in the dissociative processes of Li^+ , one geometry is disfavored for dissociation (the trigonal bipyramid, TBP), and one is favored (the wedge, W, which has the longest lifetime of the Na^+ polyhedra).

The dominant CN for the Na^+ ion is 6; however, 5 is common, and mechanistic classification of the overall exchange process for this ion, as compared to Li^+ , is much less clear-cut. Effectively, the 6-coordinated ion dissociates to form a W or SPy; however, at nearly all times, another H_2O is in position for the closest 6 waters to form a recognizable polyhedron. This suggests that the mechanism may even be I_D —dissociatively activated interchange. An argument could also be made that the ion is fractionally or 5 + 1 coordinated during the periods *moleculaRnetworks* counted CN of 5 due to the ease of association and the geometric placement of the sixth water. To form a shell with a true CN of 6, however, the H_2O must reorganize to a favored stable configuration (e.g., an octahedron). Although the high-symmetry O configuration is favorable, the Na^+ ion may have too small a surface charge density to hold it tightly. This compares favorably to the work of Chorny and Benjamin,⁶⁷ who also found both 6- and 5-coordination for Na^+ . They concluded that a dissociative mechanism is in play for the 6-coordinated species but also suggest an associative mechanism for the 5-coordinated species. Yet the data are in contrast to that observed by Spangberg et

al.,⁴⁶ who found an associative mechanism for the 6-coordinated species. As Chorny and Benjamin point out, however, the average CN is quite sensitive to the interaction parameters used in the simulation. Rey and Hynes⁶⁸ reported a most likely CN of 6, with a dissociative mechanism for exchange (they termed it “S_N1-like”), as well as complex mechanisms with some “S_N2-like” character. One curious finding of their work is that the Grote–Hynes theory they sought to employ for the rate constant broke down due to re-entry of H₂O molecules which stayed in the second shell, giving rise to a spatial dependence. We point out that the ability of *molecularnetworks* to determine the overlying 6-vertex polyhedra of the 5-coordinated Na⁺ species nearly 100% of the time offers an easily comprehended rationale for Rey’s observation. As the H₂O remain in a recognizable polyhedral structure, they are more likely to reassociate.

The MRT of waters in the first solvation shell of K⁺ is found to be 22.88, 23.88, and 25.25 ps, for an average value of 24.46 ± 1.37 ps (Table 3). Unlike Li⁺ and Na⁺ ions, the first solvation shell of K⁺ has few stable ($t > t^*$) coordination intervals. These are typically of short length, alternating with extended periods of rapid fluctuation that can be viewed as radial cutoff-dependent artifacts. As such, the (fractional) average coordination during the multiple-exchange period contributes significantly to the “true” CN reported in Table 2, and the characterization of specific mechanisms of H₂O exchange becomes less meaningful than in the other monovalent cations. Nevertheless, the same analysis was attempted for K⁺ as for Li⁺ and Na⁺. Of 261 distinct exchanges (specifically, those not immediately preceded by another fluctuation), 134 were associative and 127 dissociative reactions. These numbers are comparable to both Li⁺ and Na⁺. The following discussion focuses on the most significant exchange reactions of K⁺, which include the associative and dissociative exchange pathways of K(H₂O)₆⁺. For the associative reactions, K⁺ appears to have behavior between Li⁺ and Na⁺ since the polyhedral distribution of the oversaturated K(H₂O)₇⁺ intermediate is between that of the stable K(H₂O)₇⁺ species and the overlying polyhedra of K(H₂O)₆⁺. Specifically, the augmented trigonal prism (ATP, 26.6%), cut dodecahedron (CDo, 35.7%), and elongated trigonal pyramid (5.7%) increase in prevalence relative to the polyhedral distribution of stable K(H₂O)₇⁺, while the pentagonal bipyramid (PBP, 22.0%) and cut cube (CC, 8.7%) decrease. However, in comparison to the overlying polyhedral distribution of K(H₂O)₆⁺, the PBP is dramatically reduced in prevalence (16.2%) as is the CC (4.8%), while the capped octahedron (CO) becomes significant with 12.8% of observations. Moreover, the overlying polyhedra of K(H₂O)₆⁺ are identifiable 77% of the time, as opposed to the small number that were able to be identified for 4-coordinated Li⁺ and the near complete identification of the overlying polyhedra of 5-coordinated Na⁺. In combination, these data suggest that for a good proportion of the time the closest 7 H₂O are in a recognizable configuration around K⁺ but do need to preorganize somewhat before the seventh may enter (the CO, for example, is not conducive to addition at all), and even once it enters, the ion may not remain 7-coordinate for long due to the fluctuating nature of the shell. Seven-vertex polyhedra do not have the same level of symmetry as 6-vertex polyhedra, and it is not surprising that the most symmetric 7-coordinated geometry, the pentagonal bipyramid (PBP), is the one most frequently observed in stable periods of 7-coordination. The dissociative exchanges involving K(H₂O)₆⁺

are again an intermediate case to that observed for Li⁺ and Na⁺. There are fewer periods of stable undersaturated species, and the distribution of polyhedra within stable K(H₂O)₅⁺ is quite different from that of the underlying polyhedra of K(H₂O)₆⁺. The polyhedral distribution of the 5-coordinated dissociative intermediate falls in between the two (see Supporting Information). Temporary dissociation is more likely to involve the TBP, while stable dissociation involves the W and SPy. Although the W and SPy are stable on their own, they are also common as underlying polyhedra for 6-coordination, meaning that another H₂O could associate to form a stable 6-coordinated species without too much rearrangement of the closest 5 waters. These data reflect the ease with which H₂O enters and exits the first solvation shell of K⁺, in good accord with other literature on this ion.^{12,25,28,32} The activation barrier for exchange in K⁺ is low for both associative and dissociative exchange processes, and it is clear from the number and spread of polyhedra accessed that there are many possible pathways.

While the Mg²⁺ ion is 6-coordinate for the entire simulation period, it is useful to ask whether the under- and overlying polyhedra formed from the closest 5 and 7 waters can help to understand the stability of the first solvation shell. The dominant underlying polyhedra of Mg(H₂O)₆²⁺ is the SPy; the TBP and W are also present. That there is anything other than the square pyramid—formed by deleting any one of the vertices from the octahedron—is evidence of dynamic distortions that occur within the octahedral geometry. The lack of any 7-coordinated species within the simulation is well understood after considering the overlying polyhedra of Mg(H₂O)₆²⁺, where 7-vertex polyhedra were matched in only 81 of 40 000 snapshots—illustrating that the water molecules very rarely arrange to make 7-fold coordination possible. Clearly, were waters to exchange around Mg²⁺, the most likely pathway is dissociative, which is in agreement with NMR experiments⁵ and recently reported Car–Parrinello MD simulation.³³

The MRT H₂O in the first solvation shell of Ca²⁺ is 55.50, 69.91, and 54.63 ps, with a mean of 60.01 ± 8.58 ps (Table 3). A total of 56 distinct exchange events are observed: 34 were associative and 22 dissociative. For associative exchanges of Ca(H₂O)₇²⁺, the most commonly observed polyhedron of the oversaturated Ca(H₂O)₈²⁺ intermediate is BATP (72.1%), followed by the Do (23.8%), with the SA being rare (4.1%). This distribution is different from that of stable Ca(H₂O)₈²⁺ but similar to that of the overlying polyhedra of Ca(H₂O)₇²⁺. Of the overlying polyhedra, matches were obtained only 24.0% of the time, underlining the need for H₂O to move into position if they are to be incorporated into the first solvation shell. To be preorganized for possible associative exchange, the overlying polyhedra adopt a biaugmented triangular prism (69.8%), the dodecahedron (30.4%), and the square antiprism (0.7%). This suggests that associative exchanges take place when the molecules arrange into a recognizable 8-polyhedron, similar to Li⁺ associative exchanges. Dissociative exchange from stable Ca(H₂O)₈²⁺ yields PBP (76.5%), CO (17.6%), and CDo intermediates (5.9%). Here, it appears that dissociative exchange is more favorable when the underlying 7-vertex polyhedron has shifted to the most stable and symmetric configuration, the PBP, and the eighth water may leave without a serious shift in the shell geometry. The most common underlying 7-structure of Ca(H₂O)₈²⁺ is the CDo (56.7% of observations), a polyhedron that is much less common when the ion exists as stable Ca(H₂O)₇²⁺. The PBP is observed 41.9%

of the time for the underlying 7-coordinate structure. Upon the basis of these data, it is reasonable to conclude that there is a fundamental shift in the arrangement of the closest 7 waters when the CN changes from stable 7-coordinated to 8-coordinated species and vice versa.

The chemical mechanism of exchange for Ca^{2+} , therefore, is best described as dissociative from the dominant CN of 8. Here, the closest 7 waters of the first shell preorganize into a stable, symmetric structure such as the PBP or the CO, and the eighth H_2O is ejected. Clearly, the CDo is strongly disfavored for the ejection of the eighth H_2O , while the CO is extremely favorable. When existing at $\text{Ca}(\text{H}_2\text{O})_7^{2+}$, the shell reorganizes into CC and CDo shapes; the CDo appears to be preferred for the association of an eighth H_2O , based on its abundance as an underlying shape. It appears that once the eighth H_2O is ejected thermal fluctuation or diffusion must take place for waters to come again into position for the CN of 8 state to reform. This helps explain the slow exchange rate of Ca^{2+} and, correspondingly, the long MRT of the waters in the first solvation shell. Of the ions in this study, the hydration behavior of Ca^{2+} is one of the most difficult to study.⁵² Correspondingly, there is limited information available on the exchange mechanism. Recent QM/MM MD studies have suggested an increase in CN with increased temperature, which would imply a greater role of associative pathways. At ambient temperatures, however, the 9-coordinate species is not observed, suggesting the existence of a barrier to association that gives preference to the dissociative mechanism.

The La^{3+} ion is one of the most stable ions with respect to water exchange reactivity. The MRT is 194.23 ± 31.93 ps (Table 3). Only 15 distinct exchange events are observed in a 1 ns run, with 11 associative and 4 dissociative. The small number of events precludes a statistical comparison of polyhedral distributions regarding those with the greatest susceptibility to exchange. However, it is possible to compare the underlying polyhedral distribution of $\text{La}(\text{H}_2\text{O})_{10}^{3+}$ and the overlying polyhedral distribution of $\text{La}(\text{H}_2\text{O})_9^{3+}$ to their respective stable counterparts, and doing so reveals significant structural rearrangements tied to changes in CN. When La^{3+} is 9-coordinate, the overlying 10-vertex polyhedra is identified 82.3% of the time, and of these, 63.6% are one particular variant of the tetraaugmented trigonal prism (Tetra-ATP). Yet, when the ion is a stable 10-coordinate species, this polyhedron is observed only 3% of the time. The BCSAP, which is the dominant polyhedron adopted by $\text{La}(\text{H}_2\text{O})_{10}^{3+}$, accounts for a mere 2.8% of observations of the overlying polyhedra of $\text{La}(\text{H}_2\text{O})_9^{3+}$. The dominant underlying polyhedra of $\text{La}(\text{H}_2\text{O})_{10}^{3+}$ is the MCSAP (72%), while only 28.0% are the TATP: this is the reverse order of what is observed in stable $\text{La}(\text{H}_2\text{O})_9^{3+}$.

Thus, while the predominant polyhedron of stable $\text{La}(\text{H}_2\text{O})_9^{3+}$ is the TATP, it is rarely observed as an underlying polyhedron of the stable $\text{La}(\text{H}_2\text{O})_{10}^{3+}$ species, indicating that such a structure is highly unfavorable. Similarly, the most observed overlying polyhedron of $\text{La}(\text{H}_2\text{O})_9^{3+}$ is the tetra-ATP, not the BCSAP observed when La^{3+} is in a stable CN of 10. Moreover, it is very rare for either the stable $\text{La}(\text{H}_2\text{O})_9^{3+}$ or $\text{La}(\text{H}_2\text{O})_{10}^{3+}$ to rearrange in such a way as to promote association or dissociation to the polyhedron adopted by the exchange intermediate. The differences between the under- and overlying polyhedral distributions and their stable counterparts show, undeniably, that the coordination polyhedron of the 9-coordinate ion undergoes a dramatic shift in shape to

accommodate a tenth water into the first solvation shell and a similarly dramatic shift back to the original geometry when the excess H_2O is removed. Combined with the dominance of the 9-coordinated species, this translates into an associative mechanism for water exchange in which the tenth water, roving on the surface of the TATP, moves into a configuration that rearranges to the BCSAP. Reports on the exchange mechanisms of lanthanide ions emphasize a changeover from a dissociative pathway in 9-coordinate early lanthanides to an associative mechanism in late lanthanides, although these looked only for rotations in the coordination sphere that allowed a swap between a SAP and TTP. For lanthanum itself, there have been reports of a CN of 9.1, which matches the data presented here and suggests an associative mechanism. Here, we find no evidence of an 8-coordinated species, although we do reproduce the requirement of a significant rearrangement of the polyhedra, which Kowall et al.²³ describe in terms of a rotation of the symmetry axis and we see as a shift in the distribution of polyhedra themselves.

SUMMARY AND CONCLUSIONS

A multipronged approach has been employed to analyze prototypical MD data of aqueous alkaline, alkaline earth, and rare earth cations using the recently developed *molecularRnet-works* postprocessing R-scripts. These algorithms, some of which are graph-theoretic, characterize the instantaneous coordination environment of the metal ion in terms of the coordinating waters' H-bonding network, orientations, mean residence times, and the polyhedral structures they adopt. The extent of H-bonding and H_2O orientation is found to depend primarily upon the overall CN and the M–OH₂ distance, rather than the geometry adopted within the first solvation shell. Considering the monovalent ions, the extent of H-bonding (mean degree) increases as a function of M–OH₂ distance; however, the opposite trend is observed for the di- and trivalent ions. The strong ion–dipole interaction between H_2O and the 2+ and 3+ cations orients the H_2O dipole strongly along the O → M^{x+} vector and keep the H_2O aligned within the first solvation shell. While the H_2O closest to the ion will have the most orientational ordering regardless of ion identity, for the 2+ and 3+ cations this enhances the water's ability to H-bond with the highly ordered second shell, whereas for the monovalents, this is a penalty. The competition between the greater ability of solvating H_2O to form H-bonds when they have orientational freedom and the "optimization" of the H-bonding network with respect to angle and distance are clearly illustrated: the smaller charge on the 1+ cations means that H_2O further from the ion in the first shell will be able to rotate and H-bond with the disordered second shell, while the greater charge on the di- and trivalent cations causes their second shells to be oriented, so that the closest, most ordered waters form more H-bonds. In the second solvation shells of all ions studied, at the second maximum in the M–O pair distribution function, the H_2O are in the "best" position to H-bond with the first shell and can do so if they are aligned properly. For this reason, the mean dipole angle decreases or remains low for all ions, and then it rises as one travels through the second shell from the first-to-second shell boundary toward the second maximum in the PDF.

The polyhedral distributions indicate that those ions with the highest surface charge density have the most symmetric coordination environments, along with longer MRTs. The MRT of the lowest charge density ions is strongly affected by

the choice of t^* due to the superabundance of short coordination intervals, which, in addition, render reaction mechanisms difficult to classify. More intriguing is the investigation of correlations between the polyhedron adopted by the first solvation shell and its tendency toward aqueous exchange. A critical aspect of this analysis is the determination of the underlying and overlying polyhedra of a given CN prior to and during exchange events. In general, it is observed that Li^+ and La^{3+} favor associative exchange, while Na^+ and Ca^{2+} favor a dissociative mechanism and K^+ likely has similar activation barriers for both associative and dissociative pathways. On the basis of the polyhedron analyses, the dominant coordination environment of Li^+ and La^{3+} requires that the associating H_2O from the second solvation shell must, through thermal fluctuations, arrive at a position favorable for an association. This association leads to an oversaturated species whose underlying polyhedral distribution is different from the saturated polyhedral distribution. Dissociative exchange reactions in aqueous Ca^{2+} require a shift of the underlying polyhedron into a stable geometry necessary for dissociation. This is also true for exchange reactions about Na^+ ; however, the H_2O involved in the exchange is essentially preorganized for an exchange event to occur. The solvation shell about K^+ has such a broad distribution of shapes that it can be considered nearly amorphous and constantly shifting so that both associative and dissociative processes may occur and no simple relationship can be discerned with respect to the polyhedron adopted by the solvating waters.

■ ASSOCIATED CONTENT

● Supporting Information

Tables containing all polyhedra distributions and match percentages. This material is available free of charge via the Internet at <http://pubs.acs.org>.

■ AUTHOR INFORMATION

Corresponding Author

*E-mail: auclark@wsu.edu; lrcorral@email.arizona.edu.

Notes

The authors declare no competing financial interest.

■ ACKNOWLEDGMENTS

This work was supported in part by a grant from the Department of Energy, Basic Energy Sciences, Heavy Element program (DE-SC0001815), as well as the National Science Foundation, award # 0848346. A portion of the research was performed using EMSL, a national scientific user facility sponsored by the Department of Energy's Office of Biological and Environmental Research and located at Pacific Northwest National Laboratory.

■ REFERENCES

- (1) Lincoln, S. F.; Merbach, A. E. *Adv. Inorg. Chem.* **1995**, *42*, 1.
- (2) Helm, L.; Merbach, A. E. In *High-Pressure Chemistry*; van Eldik, R., Klarner, F.-G., Eds.; Wiley-VCH: Weinheim, 2002; p 131.
- (3) Helm, L.; Merbach, A. E. *J. Chem. Soc., Dalton Trans.* **2002**, 633.
- (4) Dunand, F. A.; Helm, L.; Merbach, A. E. *Adv. Inorg. Chem.* **2003**, *54*, 1.
- (5) Helm, L.; Merbach, A. E. *Chem. Rev.* **2005**, *105*, 1923.
- (6) Helm, L.; Nicolle, G. M.; Merbach, A. E. *Adv. Inorg. Chem.* **2005**, *57*, 327.
- (7) Marcus, Y. *Chem. Rev.* **2009**, *109*, 1346.
- (8) Brady, G. W. *J. Chem. Phys.* **1958**, *28*, 464.
- (9) Neilson, G. W.; Skipper, N. T. *Chem. Phys. Lett.* **1985**, *114*, 35.
- (10) Skipper, N. T.; Neilson, G. W. *J. Phys.: Condens. Matter* **1989**, *1*, 4141.
- (11) Jalilehvand, F.; Spangberg, D.; Lindqvist-Reis, P.; Hermansson, K.; Persson, I.; Sandstrom, M. *J. Am. Chem. Soc.* **2001**, *123*, 431.
- (12) Soper, A. K.; Weckstrom, K. *Biophys. Chem.* **2006**, *124*, 180.
- (13) Schmidt, D. A.; Scipioni, R.; Boero, M. *J. Phys. Chem. A* **2009**, *113*, 7725.
- (14) Callahan, K. M.; Casillas-Ituarte, N. N.; Roeselova, M.; Allen, H. C.; Tobias, D. J. *J. Phys. Chem. A* **2010**, *114*, 5141.
- (15) Sandstrom, J. *Dynamic NMR Spectroscopy*; Academic Press: London, 1982.
- (16) Bakker, H. J. *Chem. Rev.* **2008**, *108*, 1456.
- (17) Reuben, J.; Fiat, D. *J. Chem. Phys.* **1969**, *51*, 4918.
- (18) Reuben, J. *J. Phys. Chem.* **1975**, *79*, 2154.
- (19) Yaita, T.; Ito, D.; Tachimori, S. *J. Phys. Chem. B* **1998**, *102*, 3886.
- (20) Endom, L.; Hertz, H. G.; Thul, B.; Zeidler, M. D. *Ber. Bunsen-Ges. Phys. Chem.* **1967**, *71*, 1008.
- (21) Lee, S. H.; Rasaiah, J. C. *J. Chem. Phys.* **1994**, *101*, 6964.
- (22) Kowall, T.; Foglia, F.; Helm, L.; Merbach, A. E. *J. Am. Chem. Soc.* **1995**, *117*, 3790.
- (23) Kowall, T.; Foglia, F.; Helm, L.; Merbach, A. E. *J. Phys. Chem.* **1995**, *99*, 13078.
- (24) Lee, S. H.; Rasaiah, J. C. *J. Phys. Chem.* **1996**, *100*, 1420.
- (25) Obst, S.; Bradaczek, H. *J. Phys. Chem.* **1996**, *100*, 15677.
- (26) Koneshan, S.; Rasaiah, J. C.; Lynden-Bell, R. M.; Lee, S. H. *J. Phys. Chem. B* **1998**, *102*, 4193.
- (27) Rode, B. M.; Schwenke, C. F.; Tongraar, A. *J. Mol. Liq.* **2004**, *110*, 105.
- (28) Tongraar, A.; Rode, B. M. *Chem. Phys. Lett.* **2004**, *385*, 378.
- (29) Varma, S.; Rempe, S. B. *Biophys. Chem.* **2006**, *124*, 192.
- (30) Joung, I. S.; Cheatham, T. E. III. *J. Phys. Chem. B* **2008**, *112*, 9020.
- (31) Kerisit, S.; Rosso, K. M. *J. Chem. Phys.* **2009**, *131*, 114512.
- (32) Azam, S. S.; ul-Haq, Z.; Fatmi, M. Q. *J. Mol. Liq.* **2010**, *153*, 95.
- (33) Di Tommaso, D.; de Leeuw, N. H. *Phys. Chem. Chem. Phys.* **2010**, *12*, 894.
- (34) Impey, R. W.; Madden, P. S.; McDonald, I. R. *J. Phys. Chem.* **1983**, *87*, 5071.
- (35) Ohtaki, H.; Radnai, T. *Chem. Rev.* **1993**, *93*, 1157.
- (36) Collins, K. D.; Washabaugh, M. W. *Q. Rev. Biophys.* **1985**, *18*, 323.
- (37) Kunz, W.; Lo Nostro, P.; Ninham, B. W. *Curr. Opin. Colloid Interface Sci.* **2004**, *9*, 1.
- (38) Zhang, Y.; Cremer, P. S. *Curr. Opin. Chem. Biol.* **2006**, *10*, 658.
- (39) Zhang, Y.; Cremer, P. S. *Annu. Rev. Phys. Chem.* **2010**, *61*, 63.
- (40) Download from: <http://aclark.chem.wsu.edu/software>.
- (41) Mooney, B. L.; Corrales, L. R.; Clark, A. E. *J. Comput. Chem.* **2012**, DOI: 10.1002/jcc.22917.
- (42) Smith, W. *The DL_POLY Molecular Simulation Package*; CSE Department, STFC Daresbury Laboratory.
- (43) Aqvist, J. *J. Phys. Chem.* **1990**, *94*, 8021.
- (44) Kuta, J.; Wander, M. C. F.; Wang, Z.; Jiang, S.; Wall, N. A.; Clark, A. E. *J. Phys. Chem. C* **2011**, *115*, 21120.
- (45) Laage, D.; Hynes, J. T. *J. Phys. Chem. B* **2008**, *112*, 7697.
- (46) Spangberg, D.; Wojcik, M.; Hermansson, K. *Chem. Phys. Lett.* **1997**, *276*, 114.
- (47) Brin, S.; Page, L. In *Proceedings of the 7th International conference on the world wide web (WWW)*; Enslow, P. H., Ellis, A., Eds.; Elsevier: Amsterdam, 1998; pp 107–117.
- (48) Rudolph, W.; Brooker, M. H.; Pye, C. C. *J. Phys. Chem.* **1995**, *99*, 3793.
- (49) Loeffler, H. H.; Mohammed, A. M.; Inada, Y.; Funahashi, S. *Chem. Phys. Lett.* **2003**, *379*, 452.
- (50) Egorov, A. V.; Komolkin, A. V.; Chizhik, V. I.; Yushmanov, P. V.; Lyubartsev, A. P.; Laaksonen, A. *J. Phys. Chem. B* **2003**, *107*, 3234.
- (51) Masia, M.; Rey, R. *J. Phys. Chem. B* **2003**, *107*, 2651.
- (52) To identify the polyhedra for lithium, a longer side length had to be used. Instead of using as a cutoff the side of the largest cube fitting

inside a sphere of radius r , where r = the distance at which the first peak of the PDF = 1, the side of the largest tetrahedron fitting inside a sphere of radius r was employed. This loosened criterion makes chemical sense, as the experimentally indicated geometry of Li^+ is tetrahedral and the tetrahedron side is larger than that of the corresponding cube.

- (53) Bakker, H. J.; Skinner, J. L. *Chem. Rev.* **2010**, *110*, 1498.
- (54) Näslund, J.; Lindqvist-Reis, P.; Persson, L.; Sandström, M. *Inorg. Chem.* **2000**, *39*, 4006.
- (55) Ansell, A.; Barnes, A. C.; Mason, P. E.; Neilson, G. W.; Ramos, S. *Biophys. Chem.* **2006**, *124*, 171.
- (56) Kaufman Katz, A.; Glusker, J. P.; Beebe, S. A.; Bock, C. W. *J. Am. Chem. Soc.* **1996**, *118*, 5752.
- (57) Schwenk, C. F.; Loeffler, H. H.; Rode, B. M. *J. Chem. Phys.* **2011**, *115*, 10808.
- (58) Lim, L. H. V.; Pribil, A. B.; Ellmerer, A. E.; Randolph, B. R.; Rode, B. M. *J. Comput. Chem.* **2010**, *31*, 1195.
- (59) Shannon, R. D. *Acta Crystallogr.* **1976**, A32, 751.
- (60) Student [Gosset, W. S.] *Biometrika* **1908**, *6*, 1.
- (61) Bock, C. W.; Kaufman, A.; Glusker, J. P. *Inorg. Chem.* **1994**, *33*, 419.
- (62) Gutowski, K. E.; Dixon, D. A. *J. Phys. Chem. A* **2006**, *110*, 8840.
- (63) Kuta, J.; Clark, A. E. *Inorg. Chem.* **2010**, *49*, 7808.
- (64) Rotzinger, F. P. *J. Am. Chem. Soc.* **1997**, *119*, 5230.
- (65) Hofer, T. S.; Tran, H. T.; Schwenk, C. F.; Rode, B. M. *J. Comput. Chem.* **2004**, *25*, 211.
- (66) Loeffler, H. H.; Inada, Y.; Funahashi, S. *J. Phys. Chem. B* **2006**, *110*, 5690.
- (67) Chorny, I.; Benjamin, I. *J. Phys. Chem. B* **2005**, *109*, 16455.
- (68) Rey, R.; Hynes, J. T. *J. Phys. Chem.* **1996**, *100*, 5611.